

## 1

## Syntheses of Metal Nanocrystals

Metal nanocrystals have been extensively developed over this last two decades. Here, we will focus on spherical metal nanocrystals. We study the most important factors [1] involved to control size, size distribution, composition, and crystalline structure called nanocrystallinity. However, other parameters could emerge in the future.

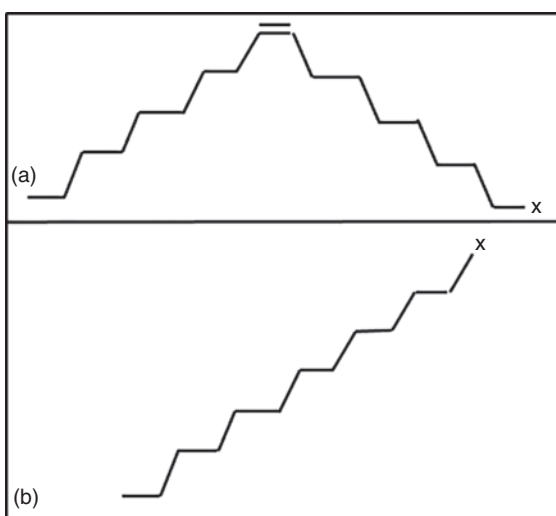
### 1.1 Nanocrystal Growth Processes and Control of Size and Distribution

The nanocrystal growth processes with control of size and size distribution have been largely studied over these past decade [1–18]. LaMer developed a theoretical model of hydrosols nucleation and growth processes [19, 20]. Ostwald observed that the atomic mobility by transfer matter from small to larger particles reduces the free energy associated with the particle/matrix interfacial area. This is called Ostwald ripening. These models have been experimented for nanoparticles/nanocrystals. The nucleation process is where nuclei (seeds) acts as templates for crystal growth. Homogeneous nucleation occurs when nuclei form uniformly throughout the parent phase, whereas heterogeneous nucleation forms at structural inhomogeneities (container surfaces, impurities, grain boundaries, dislocations). In liquid phase, heterogeneities occur much easier since a stable nucleating surface is already present. The growth of nanoparticles depends on the surface reaction and the monomer's diffusion to the surface. In many cases, the same synthesis does not produce the same final size and shape (see below). This phenomenon may be attributed to either the presence of some impurities, additives present in a very low concentration in the reactants, or sequence of reactants inducing heterogeneous nucleation. The latter is due to the changes on the growth mechanism that markedly differs with seed size and/or internal crystallinity. Consequently, various chemical methods have been developed to control the size and shape of these nanocrystals by changing the preparative conditions such as the kind and/or the amount of protecting agent.

Coating agents are needed to keep the integrity of nanocrystals. However, in reality as shown below, ligands have a vital role not only in influencing the size and size distribution of the nanocrystals but also, more importantly, in defining their interaction/interface with the environment. The ligand-mediated nanocrystal synthesis is still an open question. Actually, the role of nanocrystal/ligand differs with the metal ion and the organic ligand used. Hence, the ligand and metal nature are key parameters. At this point, we can mention the strength of ligand–nanocrystal surface interaction and the labile nature of the ligands either in the free or complex forms with the formation of clusters that it is produced with the nanocrystal constituents. The most used coating agents are surfactants. Here, we will concentrate to surfactant molecules. For most of the studies, the head polar groups are either thiol (SH), amine (NH<sub>2</sub>), or carboxylic (COOH) groups, whereas the alkyl chains are either alkane or oleic groups. In most of the cases, size selection processes are needed to produce nanocrystals with low size distribution. Carboxyl acid is covalently bound with Co and Fe atoms [21, 22]; thiol derivatives are “quasi” covalently bound to Au atoms, whereas it is lesser than Ag ones [23]. Conversely, amine groups [24] are weakly bound to most of the metallic atoms (Figure 1.1).

To control the size distribution, the digestive ripening permits to convert polydispersed to uniform nanocrystals: the first step is to break the nanocrystal large size distribution into ligand/metal complexes by ligand addition, then isolate the ligand-stabilized nanocrystals, and finally heat, at high boiling point, the solvent of the dispersed nanocrystals in the presence of ligand [25–27]. Then, the control in size and size distribution, based on van der Waals or dipolar forces, can be reached by size selection procedure. By mixing bad and good solvents for the coating agents, as obtained with polymers [28], the bad solvent for the alkyl chains induces precipitate of the largest nanocrystals, leaving the smaller nanocrystals in solution. After centrifugation, the precipitate is dissolved with a good solvent for the alkyl chains,

**Figure 1.1** Various coating agents used to coat nanocrystals: (a) oley group (C<sub>18</sub>H<sub>36</sub>X) and (b) alkyl chains (C<sub>12</sub>H<sub>25</sub>X). X is the head polar group: X = SH thiol derivatives, X = COOH acid derivatives, and X = NH<sub>2</sub> amine derivatives.



leading to a homogeneous clear solution, and again a bad solvent is added inducing a new precipitate. Similarly, the supernatant solvent is evaporated, and the same procedure as the precipitate is proceeded. Such process is repeated several times before reaching a sufficient low size distribution ( $\leq 10\%$ ) and consequently to be able to self-assemble in 2D or 3D superlattices. A rather large number of mixed solvents is used to size select nanocrystals: the solvent/nonsolvent pairs for the coating agent, e.g. hexane/ethanol, heptane/ethanol, chloroform/ethanol, chloroform/methanol, and pyridine/hexane, are usually used. Ligands, considered as capping/passivating agents, play a major role in the control of nanocrystal size and is far from only providing stability to the nanocrystal against aggregation.

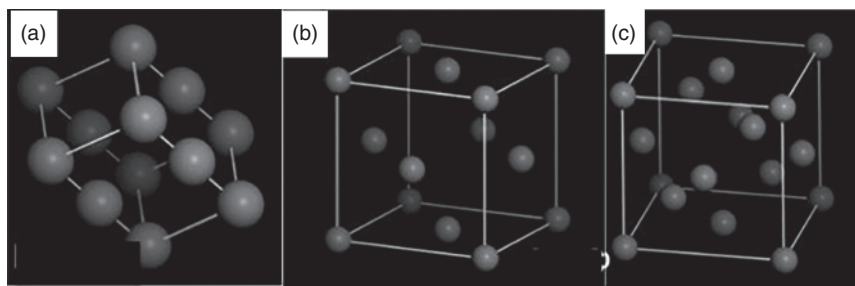
With the most used syntheses to produce well-defined metal nanocrystals with a very low size distribution, several procedures are used: reverse micelles, inorganic chemical reaction, hot injection processes, and thermal decomposition. They are based on chemical reduction of the metal ion by various reducing agents such as hydrazine, sodium borohydride ( $\text{NaBH}_4$ ), citrate, and glycol. The control of nanocrystal size depends on (i) the relative concentrations of the reactants, (ii) the coating agent concentration, (iii) the structure of the coating agent, (iv) the relative amount of reactant and that of the coating agent (the higher the stabilizer agent compared with reactants, the smaller nuclei formed and consequently smaller nanocrystal size), and (v) the mixture of two coating agents (one binds tightly to the nanocrystal surface hindering growth, and the other less tightly bound favors the rapid growth).

## 1.2 Crystalline Structure of Metal Nanocrystals

Generally, the nanocrystal size is determined by the number of atoms produced and consequently by the number of the nanoparticles formed depending on the kinetics of nucleation and growth processes. The nanocrystal crystalline structure called nanocrystallinity is determined by the competition between the kinetics of structural transformation of the nanoparticles and that of delivering separation between nucleation/growth processes (e.g. a burst of nucleation) and diffusion-controlled growth [29–34].

### 1.2.1 Co Nanocrystals

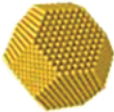
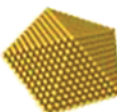
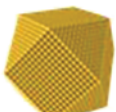
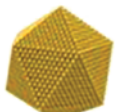
Cobalt has three nearly isoenergetic crystal structures (Figure 1.2): hexagonal close-packed (hcp), face-centered cubic (fcc), and epsilon ( $\epsilon$ ). Bulk cobalt displays two stable phases of hcp and fcc at ambient pressure. At the nanoscale, it can possess the epsilon phase with a complex cubic primitive structure, which is similar to that of  $\beta$ -manganese, with a unit cell parameter of  $6.097 \text{ \AA}$  [35]. This metastable crystal structure ( $\epsilon$  phase) can be transformed to hcp or fcc structure by annealing the sample at a suitable temperature [36]. Due to its relatively smaller magnetocrystalline anisotropy constant ( $K_c \approx 1.5 \times 10^5 \text{ J m}^{-3}$ ),  $\epsilon$ -structure is widely known as a softer magnetic material, compared with the hcp and fcc phases.



**Figure 1.2** Crystalline structures of Co nanocrystals (a) hcp, (b) fcc, and (c)  $\epsilon$ -phase.

### 1.2.2 Au, Ag, and Cu Nanocrystals

At the atomic level, the densest possible packing of four spheres is a tetrahedron [29, 37–39]. At the earliest stages of growth of a solid, the atoms reorganized into a completely new structure each time an atom is added. For fcc materials, the nanocrystals considered as compact packing of spheres are cuboctahedra, decahedra, and icosahedra (Figure 1.3). The surface of a cuboctahedral nanocrystals consisted of eight (111) planes and six (100) planes with closed atomic shells and represents the most stable form. The defined number of atoms resulted exclusively from the geometric arrangements and cannot be explained by the electronic shell model. The decahedra and icosahedra are structures with fivefold symmetry and are called multiple-twinned particles (MTPs). In fact, decahedral nanocrystals consisted of five deformed tetrahedral subunits twinned by their {111} planes, whereas icosahedral clusters originated from the twinning of 20, (111) faces, deformed tetrahedral subunits.

Single crystals	Polycrystals
 Truncated octahedra	 Decahedra
 Cuboctahedra	 Icosahedra

**Figure 1.3** Various shapes of fcc nanocrystal arrangements.

## 1.3 Various Techniques Used to Produce Metal Nanocrystals and Control Their Sizes and Distribution

A very large number of techniques have been used to produce nanocrystals, with very low size distribution. Significant advantages of methodologies using high-boiling-point solvents and organometallic precursors in the presence or absence of surfactants favor the control of nanoparticles size and improve the crystalline structure of the nanocrystals [11, 33, 40].

### 1.3.1 Reverse Micelles

Reverse micelles [2, 17, 41–48] are well known water-in-oil droplets stabilized by surfactants [49]. The best surfactant providing uniform droplets is sodium bis(2-ethylhexyl)sulfosuccinate, Na(AOT), called Aerosol OT. The amount of water controls the droplet size (Figure 1.4a). The average droplet diameter increases linearly with the water content,  $w$ , defined as  $w = [\text{H}_2\text{O}]/[\text{AOT}]$ . By collisions these droplets exchange their water contents and form again two independent droplets (Figure 1.4b). This process is used to produce nanosized material by either chemical reduction of metal ions or coprecipitation reactions. At low water content, the number of water molecules per surfactant is too small to hydrate the counterions and the head polar groups. This induces strong interactions between water molecules and the head polar groups. This induces strong interactions between water molecules and the head polar groups. The water molecules are then considered as “bound water.”

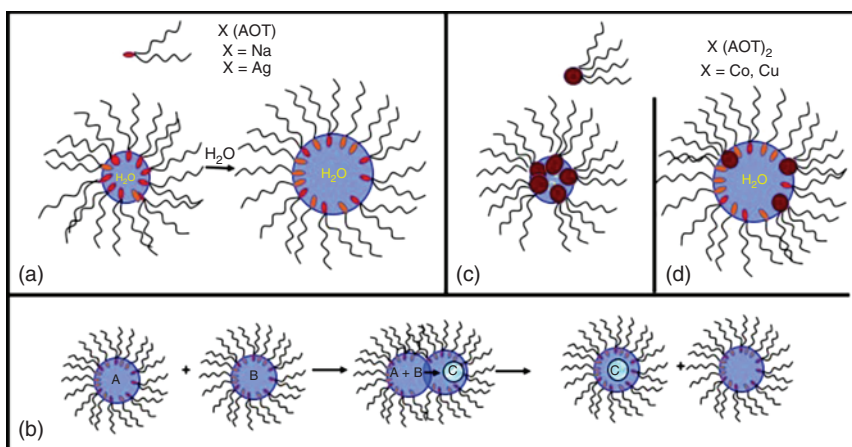


**Figure 1.4** (a) Control the size of the droplet with the amount of water with Na bis(2-ethylhexyl)sulfosuccinate, Na(AOT). Similar behavior is observed with Ag(AOT). (b) Exchange process by collision between two droplets to favor chemical reaction. (c) Reverse micelles from functionalized surfactant Co and Cu (tetra (2-ethylhexyl) sulfosuccinate),  $\text{X}(\text{AOT})_2$ . (d) Mixed micelles.

An increase of the water content induces a progressive appearance of “free” water molecules in the center of the droplets, whereas some of water molecules remain bound to the interface. With Na(AOT), the bulk water phase is reached around  $w = 10$ . To produce metal nanocrystals without any oxide formation, the metal ions have to be in environment of bound water molecules and not into the bulk phase, i.e. they have to be located at the oil–water interface of the droplets. This explains why we synthesized functionalized surfactants  $X_n(\text{AOT})_n$  with  $n = 1$  or 2, i.e. the sodium ions of AOT are replaced by metallic ones (Figure 1.4c). With  $X_n(\text{AOT})_n$ , reverse micelles are formed to produce reverse micelles, but the amount of water inside reverse micelles is limited ( $w \neq 5$ ) [42]. To provide a control of the droplet size by the water content, we used mixed micelles, Na(AOT),  $X_n(\text{AOT})_n$ . In such condition, the size of the droplet remains controlled by the amount of water molecules involved in the formation of reverse micelles that can then play the role of template (Figure 1.4d).

To synthesize amorphous Co nanoparticles, mixed micelles  $[\text{Co}(\text{AOT})_2/\text{Na}(\text{AOT})]$  are used. Sodium borohydride ( $\text{NaBH}_4$ ) added to the micellar solution reduces the cobalt ions. Immediately after  $\text{NaBH}_4$  addition, the color of the micellar solution changes from pink to black, indicating the formation of colloidal Co nanoparticles. Coating agents with carboxylic as head group dodecanoic acid molecules added to the colloidal solution induce a chemical bond between the oxygen of carboxyl group and the Co atoms located at the interface. The coated Co nanoparticles are then washed and centrifuged several times with ethanol to remove all the AOT surfactant. Moreover, the black powder obtained is dispersed in hexane, and the colloidal solution is isotropic. Size selection process as described above takes place to produce Co nanoparticles with a  $\sim 10\%$  size distribution. The entire synthesis is carried out in an  $\text{N}_2$  glove box using de-oxygenated solvents to prevent nanoparticle oxidation. The ratios of  $[\text{NaBH}_4]/[\text{Co}(\text{AOT})_2]$  and  $[\text{Na}(\text{AOT})]/[\text{Co}(\text{AOT})_2]$  control the nanoparticle size. In contrary to others, the nanoparticles are amorphous. The average diameter and size distribution evolve from 4 to 9 nm and 9% to 13%, respectively (Figure 1.5a). The relative ratio between Na(AOT) and  $\text{Co}(\text{AOT})_2$  controls the nanoparticle size. By annealing process, under an inert atmosphere, the crystalline structure of Co nanoparticles is improved, and a transition from amorphous to single-domain hcp structure takes place [47, 48]. The annealing process does not significantly affect the nanocrystal diameter and its size distribution.

Amorphous Co nanoparticles deposited on the TEM grid are annealed under inert gas, 60 minutes at  $250^\circ\text{C}$ . During such process, as shown in Figure 1.6, a transition of the crystalline Co nanoparticles from amorphous to single-domain hcp phase takes place. Note the hcp nanocrystal size increases compared with the corresponding amorphous counterparts. This is due to hcp lattice fringes. Hence, the crystallinity of Co nanoparticles is controlled by keeping the other parameters constant as size and surface coating. The control of amorphous Co nanoparticle size is obtained by mixing Na(AOT) with  $\text{Co}(\text{AOT})_2$  [50].

To produce Ag nanocrystals by using reverse micelles, a colloidal solution of Na(AOT) and Ag(AOT) is mixed with Na(AOT) reverse micelles containing hydrazine [51]. The nanocrystals are extracted from the micellar solution and then are



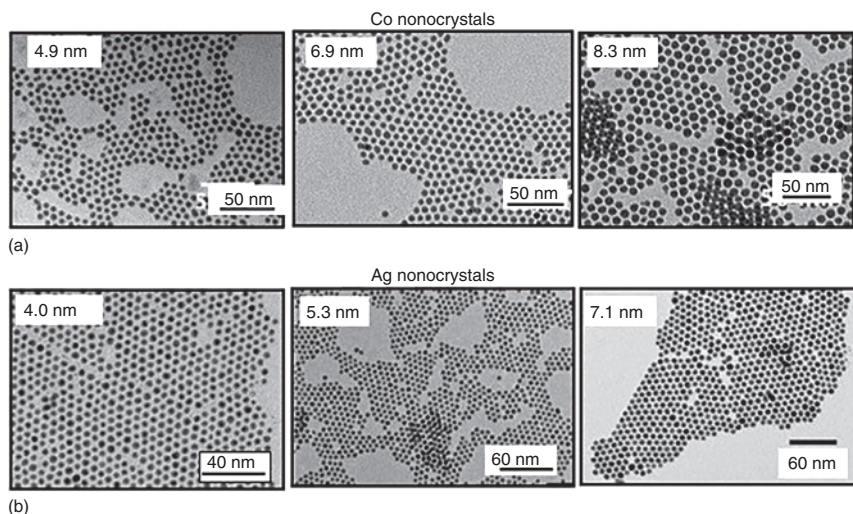


**Figure 1.5** (a) Increase in the size of Co nanoparticles with controlling  $R$ ,  $w$ , and the relative amount of  $\text{Co}(\text{AOT})_2$ . (b) Reduction of mixed reverse micelles of  $\text{Ag}(\text{AOT})/\text{Na}(\text{AOT})$  (6/4) by hydrazine with  $w = 2$ . By controlling the ratio  $R = [\text{Ag}(\text{AOT})]/[\text{hydrazine}]$  from 4 to 0.7, the Ag nanocrystal sizes are (a) 4, (b) 5, (c) 6, and (d) 7 nm, respectively.

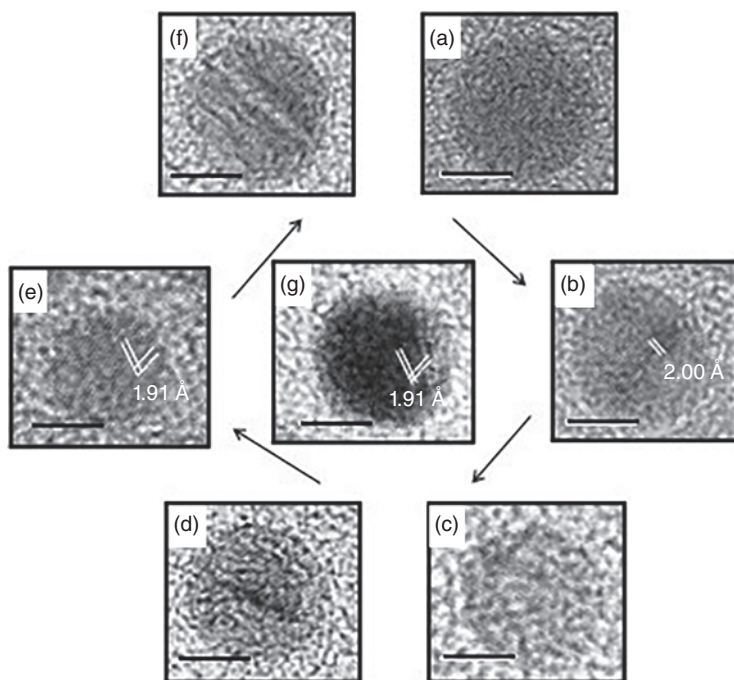


**Figure 1.6** Schematic illustration with high-resolution TEM (HRTEM) images of the evolution process of 7.2-nm Co nanocrystals: (a) amorphous Co nanoparticles, (b) hcp Co with large domains, (c) and (d) very large domains, (e) small hcp single crystals, (f) hcp single crystals with stacking faults, and (g) hcp single crystals. The scale bar is 3 nm. Source: Yang et al. [48]/American Chemical Society.

subjected to the ethanol/hexane wash cycles. Changing the water content and the ratios of  $[\text{Ag}(\text{AOT})]/[\text{hydrazine}]$  and  $[\text{Ag}(\text{AOT})]/[\text{Na}(\text{AOT})]$  controls the Ag nanocrystal from 4 to 7.3 nm (Figure 1.5b).

### 1.3.2 Inorganic Chemical Reaction to Produce Au and Ag Nanocrystals

#### 1.3.2.1 Synthesis of Au Nanocrystals Differing by Their Diameters

Au nanocrystals are synthesized by revisiting the Stucky method [51–54]: two solutions (A) and (B) are mixed under nitrogen protection. (A) is a preheated solution of chlorotriphenylphosphine Au(I) dissolved in toluene containing dodecanethiol, and (B) is amine–borane complex dissolved in toluene. The ratio of the volume of A/B controls the size of the nanocrystals from 7.8 to 5.8 nm. To decrease the size from 5.1 to 4 nm, the solution B is replaced by *tert*-butylamine and ammonia borane complexes, respectively (Figure 1.7). For simplicity, details on the synthesis to control the nanocrystal size are given in Table 1.1.

Let us consider 5-nm Au nanocrystals: at the end of an organometallic synthesis, a drop of Au nanocrystals dispersed in toluene is deposited on TEM grid. The dark-field TEM image (Figure 1.8) shows homogeneous or inhomogeneous contrasts corresponding to single and polycrystalline nanocrystals, respectively. After analyzing

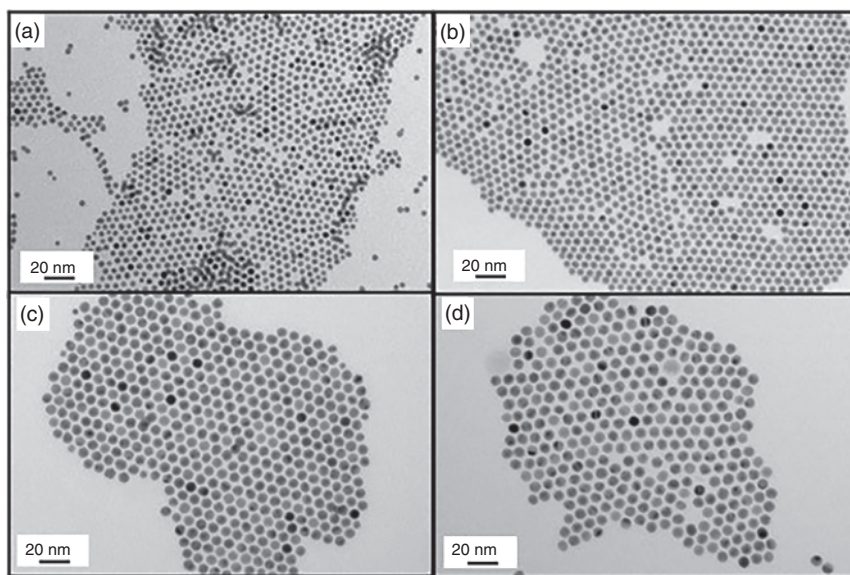


**Figure 1.7** TEM image and corresponding histograms of 4 (a), 5 (b), 7 (c), and 8 nm (d) obtained by deposition of a drop of colloidal solution of Au nanocrystals coated with dodecanethiol and dispersed in toluene. Source: Goubet et al. [55]/JOHN WILEY & SONS, INC.



**Table 1.1** Experimental conditions to produce Au nanocrystals differing by their average diameters.

Diameters (nm)	4.3	5.1	5.8	7.2	7.8
$\sigma$ (%)	9	7	8	6	6
$V_{\text{doc}}$ ( $\mu\text{l}$ )	500	500	500	125	125
$N_{\text{bo}}$	2.5	5	5	5	10
$S$	Et/TO	TO	TO	TO	TO

Solutions A and B are 0.25 mmol of chlorotriphenylphosphine Au(I) and *tert*-butylamine borane complex dissolved in 25 ml toluene, respectively.  $D$ ,  $s$ ,  $V_{\text{doc}}$ ,  $N_{\text{bo}}$ ,  $S$ , Eth, and To are the Au nanocrystal diameter, size distribution, the volume of dodecanethiol in 25 ml solution, the amount in mmol in 2 ml of solution, solvent, ethanol, and toluene, respectively.

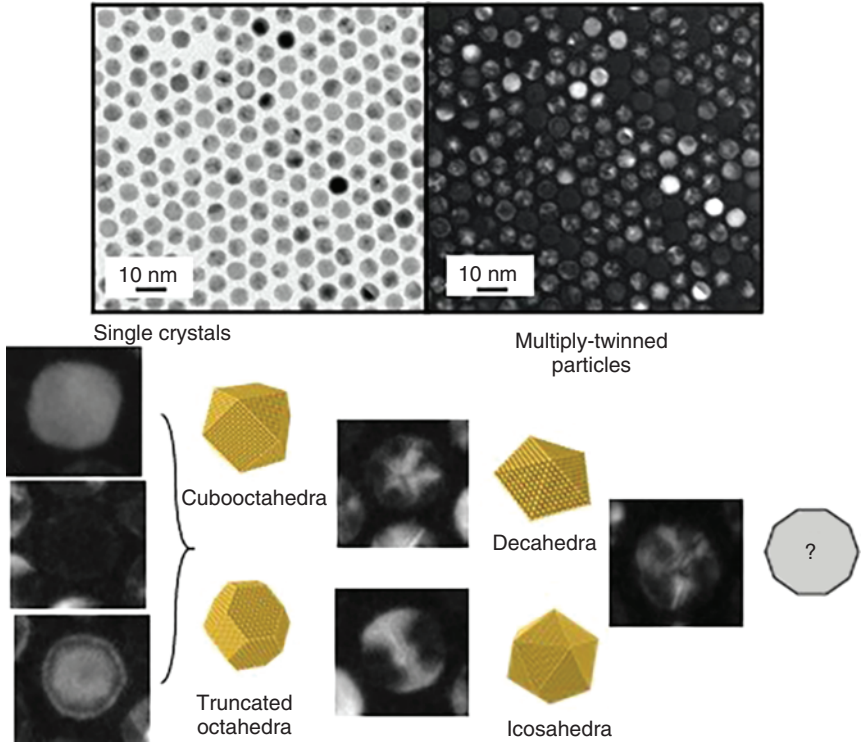


**Figure 1.8** Bright- and dark-field TEM image of 5.1-nm Au nanocrystals with homogeneous (single-domain) and heterogeneous (polycrystal) contrasts. Source: Portalès et al. [56]/American Chemical Society.

the conical dark-field TEM images over a total population of 2000 nanocrystals, the amount of single-crystalline nanocrystals is found to be approximately 30% of the full population. The major portion (65%) is composed of MTPs and/or polycrystals, while 5% is poorly twinned nanocrystals. On increasing the Au nanocrystals size, the amount of single domain markedly decreases.

In Chapter 4, we describe nanocrystal segregation processes with the formation of interfacial and precipitate 3D superlattices by subjecting colloidal solution to toluene-saturated atmosphere after keeping during seven days. Both interfacial and precipitate 3D superlattices are characterized by single-domain 5-nm Au nanocrystals, whereas the corresponding polycrystalline phase remains in solution [54]. This crystalline selection process makes possible to select 5-nm single-domain and polycrystalline nanocrystals. The growth of the seeds is induced in a solution of Au–oleylamine complex, produced by mixing  $\text{HAuCl}_4$  in pure oleylamine [57]. After dissolution, the solution is yellow colored and freshly used. Then, colloidal solutions of either single-domain (Figure 1.9a) or polycrystalline (Figure 1.9f) 5-nm nanocrystals are mixed with the Au–oleylamine complex solution, and the volume is completed with toluene. The seeded growth takes place at fixed temperature. During a few hours, Au–oleylamine complex is slowly reduced on the seeds. Adjusting the gold complex concentration can control the resulting nanocrystal size. After reaction, the nanocrystals are washed with ethanol and redispersed in chloroform.

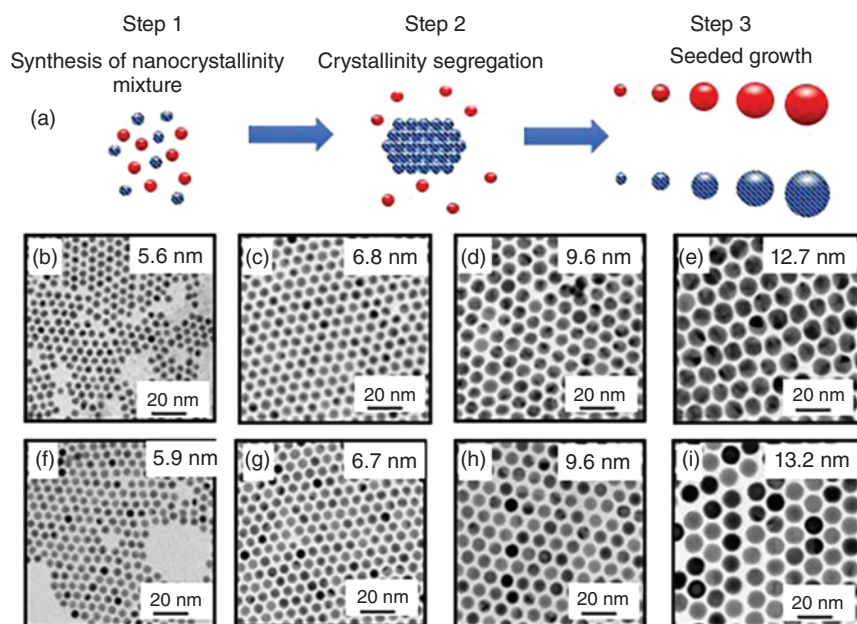


**Figure 1.9** (a) A schematic image showing the formation of Au nanocrystals with tunable size and nanocrystallinity. The polycrystalline nanocrystals are represented in red, and single-domain nanocrystals in blue with straight lines. (b–e) TEM images of NPs synthesized using polycrystalline seeds: (b) 5.6, (c) 6.8, (d) 9.6, and (e) 12.7 nm. (f–i) TEM images of NPs synthesized using single-domain seeds: (f) 5.9, (g) 6.7, (h) 9.6, and (i) 13.2 nm. The scale bars are 20 nm. Source: Goubet et al. [57]/Royal Society of Chemistry.

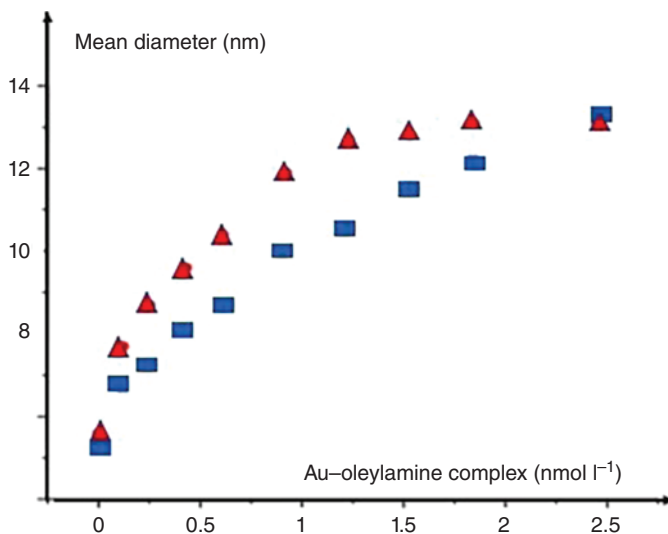


**Figure 1.10** Typical mean diameter of single-domain (blue squares) and polycrystalline (red circles) nanocrystals as a function of gold complex concentration during the seeded growth. Source: Goubet et al. [57]/Royal Society of Chemistry.

Hence, the control of nanocrystal size from 5 to 13 nm is obtained with either single-domain (Figure 1.9b–e) and polycrystalline (Figure 1.9f–i) nanocrystals.

Figure 1.10 shows the increase in the seed growth that is rather fast for polycrystalline nanocrystals compared with the corresponding single nanocrystals. By tuning the Au-oleylamine concentration, the control of mean diameter can be reduced to 0.5 nm.

### 1.3.2.2 Synthesis of 5-nm Polycrystalline Silver Nanocrystals

Same procedure as described above is developed [51]. The precursor chlorotriphenylphosphine gold(I) is replaced by its Ag counterparts [chlorotris(triphenylphosphine) silver]. A solution of this precursor is mixed with dodecanethiol. A solution of *tert*-butylamine borane complex at 0.17 M is then added for the reduction. After few hours, some small particles (<2 nm) start to appear in the solution and progressively. After leaving the solution to stir overnight, nanocrystals with the diameter of 5.1 nm having very narrow size distribution are obtained (Figure 1.11).

### 1.3.3 Thermal Decomposition

The thermal decomposition process has been well developed to produce a rather large number of metal and metal oxide nanoparticles [18, 36, 59]. Hence, cobalt carbonyl ( $\text{Co}_2(\text{CO})_8$ ) is dissolved in dioctylamine in the presence of oleic acid to produce fcc Co nanocrystals (Figure 1.12). By adjusting the ligand concentration and decomposition temperature, the multidomain fcc Co nanocrystals having a diameter of 5–10 nm with a rather low size distribution (from 7% to 10%) are produced.

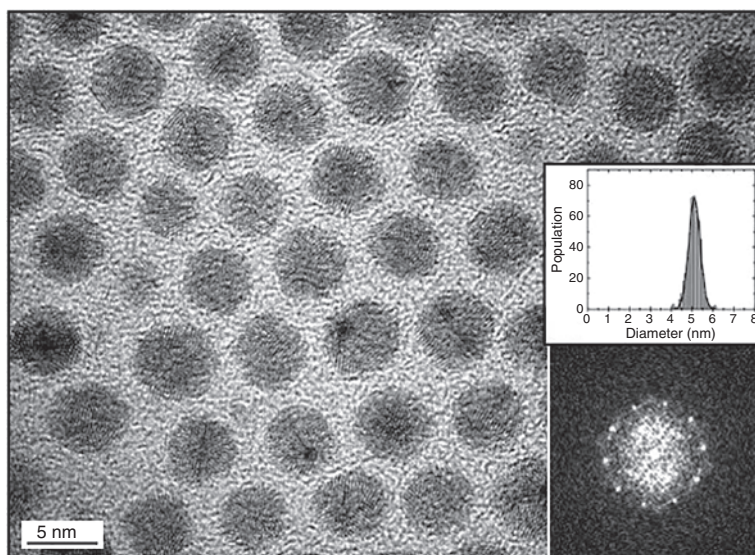


**Figure 1.11** HRTEM characterization of silver MTPs. HRTEM image and size distribution histogram of multiply twinned 5.1 nm Ag nanocrystals. Inserts: The size distribution histogram is determined from over 500 silver nanocrystals from the colloidal solution used and power spectrum as typically obtained from a silver icosahedron oriented along the fivefold axis. Source: Portalès et al. [58].

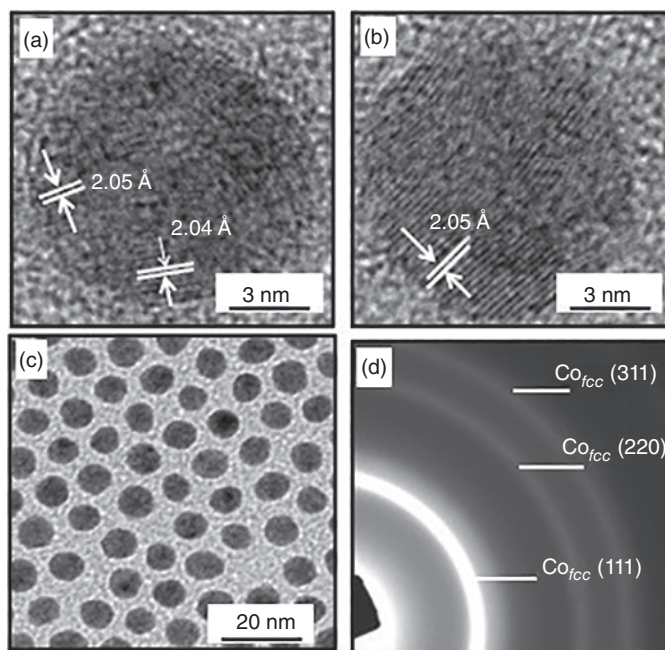


**Figure 1.12** HRTEM (a, b) and TEM (c) images and electron diffraction pattern (d) of fcc Co nanocrystals produced as described above. Engineering the magnetic dipolar interactions in three-dimensional binary supracrystals via mesoscale alloying. Source: Yang et al. [60]/John Wiley & Sons.



### 1.3.4 Hot Injection

This method is based in injection of a cool solution of precursor molecules into hot liquid [4, 35, 61–63]. The injection leads to the instantaneous formation of seeds. The decrease of solvent temperature prevents the formation of new nuclei. The reactant container is a suspension of reasonably rather homogeneous nuclei together with considerable amounts of precursors. To slow the growth of the existing nuclei without any new nucleation, the solution is heated below the corresponding injection temperature. The omnipresent ligand molecules slow down the growth considerably by coordinating the surface atoms, thus forming a steric barrier for reactants. The slow growth at relatively high temperatures allows the nanocrystals to anneal and to form nearly single-domain lattices at the same distance as those of the bulk phase. At the end of the syntheses, size selection takes place by the addition of a non-solvent to reach low size distribution. The ligands remain attached to the surface atoms, and the suspensions are sterically stabilized. The nanocrystal size increases with temperature to which the nuclei grow. Note that another approach is a rapid injection in hot water of the reactants [64].

Single-domain  $\epsilon$ -phase Co nanocrystals are produced by hot injection: a mixture of trioctylphosphine oxide (TOPO), oleic acid, and (1,2-dichlorobenzene) DCB is heated to under flowing nitrogen.  $\text{Co}_2(\text{CO})_8$  dissolved in DCB is quickly injected in the solution under vigorously stirring. The rapid injection of the cobalt complex into hot organic solution can minimize the nucleation stage, inducing burst nucleation of Co monomers. The solution is held at high temperature and then cooled down to room temperature. The as-prepared nanocrystals are isolated by adding anhydrous ethanol. Comparison of bright- and dark-field images of homogeneous dark or bright nanocrystals (Figure 1.13a,b) indicates the formation of single-domain nanocrystals (Figure 1.13). The high-resolution TEM image and the diffraction pattern (Figure 1.13c,d) confirms the formation of single domain of  $\epsilon$ -phase Co nanocrystals. The number of nuclei formed in the hot injection synthesis of  $\epsilon$ -Co nanocrystals depends more on temperature kinetics after the injection than on the injection itself [65]. This indicates a faster recovery of temperature after injection leading to smaller-sized nanocrystals. The size of Co nanocrystals is tuned, from 5 to 10 nm, by adjusting both concentration of oleic acid and temperature.

This hot injection method is used to produce Ag nanocrystals coated with oleylamine ( $\text{C}_{18}\text{-NH}_2$ ) and dodecylamine ( $\text{C}_{12}\text{-NH}_2$ ). Briefly,  $\text{AgNO}_3$  and dodecane diol are separately dissolved in *o*-dichlorobenzene (DCB). These solutions are called A and B, respectively, for simplicity. A is rapidly injected into a hot B solution. The mixture reacts in few minutes. The solution is then cooled down to room temperature. With oleylamine ( $\text{C}_{18}\text{-NH}_2$ ), this procedure produces the Ag nanocrystal size from 2.2 to 7 nm, (Figure 1.14). The change of the nanocrystals is obtained by changing the relative ratio of  $\text{AgNO}_3$  and oleylamine. For larger nanocrystal size (from 8 to 13 nm), oleylamine-coated nanocrystals are prepared following a modified one-pot method as described elsewhere [8].

Hence, this procedure permits to control the nanocrystal size from 2 to 13 nm. The TEM images in Figure 1.14 clearly show that the nanocrystals, regardless of their size, are well arranged in a two-dimensional hexagonal close-packed array. This is typical of

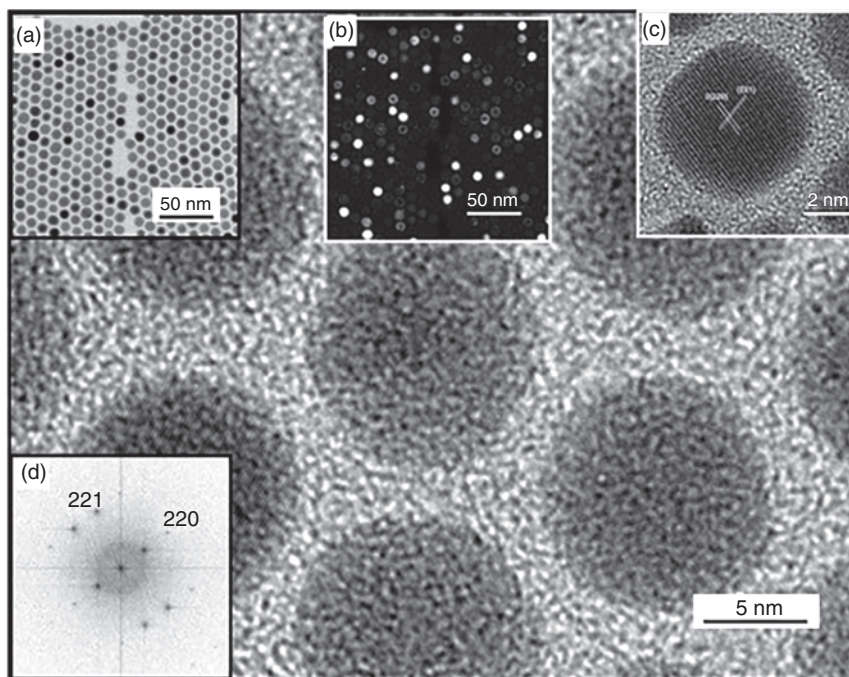


**Figure 1.13** High-resolution of TEM images of 7.6-nm  $\epsilon$ -phase Co nanocrystals, long range TEM images bright (b) and conical dark field (c), high-resolution TEM image of isolated nanocrystal (d), and corresponding electron diffraction pattern (e). The  $\epsilon$ -phase Co nanocrystals are produced with OA/TOPO = 2.4.

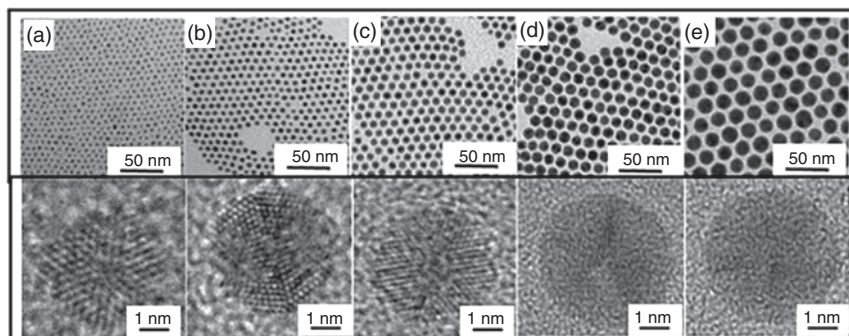


**Figure 1.14** TEM images and high-resolution TEM of oleylamine-coated silver NCs produced by either hot injection (a–c) or one-pot method (d, e): (a) 2.2, (b) 4.1, (c) 5.9, (d) 8.7, and (e) 12.9 nm.

nanocrystals with low size distribution (typically below 10%). Note that these nanocrystals are obtained without any post-synthesis size selection process or size-focusing ripening process. This is, from the best of our knowledge, the first report of Ag nanocrystal preparation with such a low size distribution. High-resolution TEM images of the nanocrystals reveal that all nanocrystals are MTPs with icosahedral morphologies. Replacing oleylamine ( $C_{18}\text{-NH}_2$ ) by dodecylamine ( $C_{12}\text{-NH}_2$ ), which is a similar



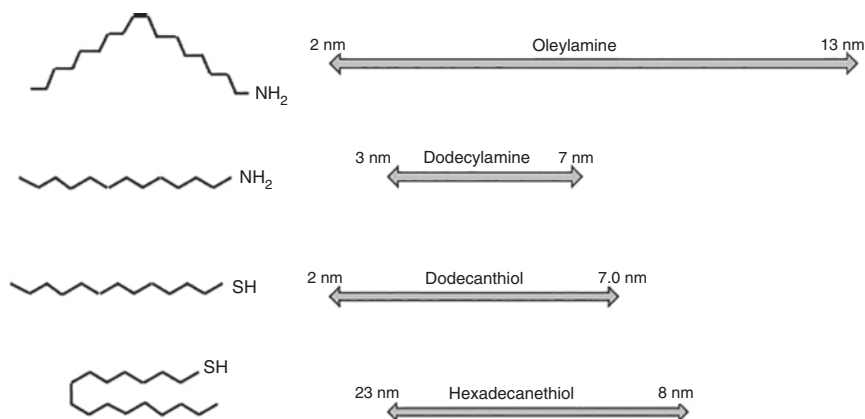


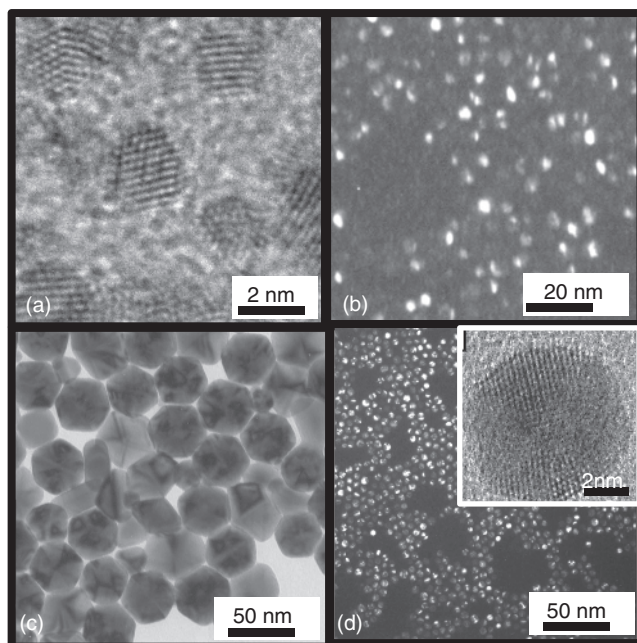
**Figure 1.15** Average size of Ag nanocrystals produced by the same procedure and coated with various coating agents.

$-\text{NH}_2$ -terminated coating agent with a shorter alkyl chain, stable Ag nanocrystals are produced. In this case, the size of the dodecanethiol-coated Ag nanocrystals is controlled from 3.0 to 6.3 nm. Again, the size distribution of these nanocrystals is kept below 10% without the need of size segregation procedures. Such hot injection process cannot be used for the preparation of alkanethiol-coated Ag nanocrystals since  $\text{AgNO}_3$  cannot be dissolved in DCB in the presence of  $-\text{SH}$ -terminated coating agent. When a mixture of  $\text{AgNO}_3$  and dodecanethiol ( $\text{C}_{12}-\text{SH}$ ) is injected into hot solutions containing polyols, small nanocrystals with large size distribution are produced. Hence, to obtain Ag nanocrystals having similar sizes with a new coating agent such as alkanethiol, the ligand exchange process from nanocrystals coated with oleylamine is used. The colloidal solution of Ag nanocrystals coated with oleylamine is mixed with a small amount of  $\text{C}_{12}-\text{SH}$ ; the mixture is kept under vigorous stirring. Hence, this method is highly powerful to control the size and size distribution ( $<10\%$ ) without any other complementary processes to reduce the size distribution. However, the size range of nanocrystals depends on the coating agent (Figure 1.15).

## 1.4 An Example to Show the Importance of the Reactant Sequence to Produce Nanocrystals

Here, we will show how the sequence of reactants plays a key factor in the final size of Au nanocrystals [13]. By revisited Brust method [66, 67] to produce Au nanocrystals coated with dodecanethiol, the coating agent is added to the reactant ( $\text{HAuCl}_4 \cdot 3\text{H}_2\text{O}$ ) either before or after the chemical reduction. The addition of  $\text{C}_{12}-\text{SH}$  before the chemical reduction induces the formation of polymeric Au(I) thiolate species. At the end of the synthesis, rather small single-domain nanocrystals with an average diameter of 1.5 nm and a size distribution of 25% are produced (Figure 1.16a). When  $\text{C}_{12}-\text{SH}$  is added at the end of the synthesis, 3.5-nm MTP nanocrystals with 20% size distribution are obtained (Figure 1.16b). Hence, the size of the nanocrystals

**Figure 1.16** TEM image of nanocrystals produce by dodecanethiol addition. Before (a) and after (b) addition of the reducing agent. By thermal treatments of (a) and (b) dispersed in toluene, the final products are (c) and (d), respectively. Source: Goubet et al. [13]/ American Chemical Society.



is controlled by the sequence of reaction additions. These two nanocrystals (1.5 and 3.5 nm) considered as seeds (I and II, respectively) are dispersed in toluene and subjected to the same thermal treatment at 463 K during the same period of time [68]. At the end of the process, seed I produced very well-faceted hexagonal particles (85%) and triangular (9%) and pentagonal (6%) Au nanocrystals (Figure 1.16c). Thus, thermal treatment of 1.5-nm cuboctahedral Au nanocrystals induces the formation of large icosahedral particles. With 3.5 nm as seed (II), 5.8-nm Au nanocrystals with 9% size distribution are produced (Figure 1.16d). This is explained as follows: small cuboctahedra (1.5 nm) subjected to thermal treatment melt and reach a liquidlike phase. This leads by slow cooling rate to the formation of mainly large icosahedral particles that are the most stable Au fcc structures and the presence of small amounts of other structures. By simulation [69, 70], it is found that crystallization of the interior and external atoms leads to an icosahedral structure. The discovery of, at equilibrium, the Au nanoparticles consisting of 85% icosahedral particles is explained by the low surface energy of Au(111) surface [69]. This confirms that the kinetics of nucleation and growth in clusters play a key role in determining the structure of the nanocrystals. The stochastic nature of nucleation explains why other shapes are produced as well. Conversely, when the seed size is larger, they no longer melt, and migration of atoms/adatoms between nanocrystals becomes the predominant growth and shaping mechanism [69, 71].

## 1.5 N-Heterocyclic Carbene Ligands for Au Nanocrystals Stabilization

N-Heterocyclic carbenes (NHCs) [72–80] have attracted increasing attention as neutral C-ligands for nanomaterial stabilization and functionalization [81–103]. The NHC high flexibility allows fine-tuning of steric and electronic properties and facilitates the introduction of functional groups at different positions [104]. The N-substituents of the NHCs point out from both sides and are oriented toward the metallic surface, inducing significant interactions with the metallic surface and the neighboring ligands. Therefore, NHC structure modulations can dramatically affect the NHC bonding mode, the surface covering and ligand packing density, and the number of free metallic sites available for catalysis. Furthermore, the strong  $\sigma$ -donating properties of NHCs are expected [105], as in metal complexes [106], to provide strong NHC–metal bonds at the surfaces. The most commonly used method for obtaining NHCs involves deprotonation of the precursor azolium salts [105]. In contrast to many metal–NHC complexes, free NHCs are highly sensitive to oxygen, water, and carbon dioxide and should be handled with exclusion of air and moisture. In many experimental procedures, NHCs and metal-ligated NHCs are generated *in situ* under inert atmosphere [72, 73]. Various synthetic methods have been tested for the formation of metal (M) NCs stabilized by NHC ligands (M = Ir, Ag, Au, Ru, Pd, Pt) [81–99]. Some NHC-based metal NCs have been applied in metal-catalyzed hydrogenation reactions (M = Ir, Ru, Pd, Pt) [82, 88–90, 92, 99]. The enhanced stability of NHC-based SAMs and NCs to oxidative treatments was reported [100, 101].

Two new methods are proposed to produce Au nanocrystals coated with various NHC ligands as described in Figure 1.17 [76–80]:

- (i) *One-phase reduction method*: the control of nanocrystal size and stability is the first major challenge when new ligands are introduced. Previous study shows one-phase procedure to produce Au nanocrystals with triphenylphosphine gold chloride in the presence of an excess of dodecanethiol as described in Section 1.3.2.1 [54, 107]. Let us consider similar approach by using [(NHC)AuCl] complexes. Ammonia–borane complex ( $\text{NH}_3\text{BH}_3$ ) in toluene at 100 °C is used as reducing agent (Figure 1.17). The best data are obtained with **5** ligand as precursor. Au nanocrystals with an average size of 9.8 nm and a narrow size distribution of  $\pm 6.9\%$  are produced. However, a limited long-term stability was observed for **L5@Au** nanocrystal that precipitates from the toluene solution after 12 hours. Hence, NHC can play a dual role both as a ligand for the initial  $\text{Au}^{\text{I}}$  species and as a stabilizing agent for the metallic NCs formed (Figure 1.18).

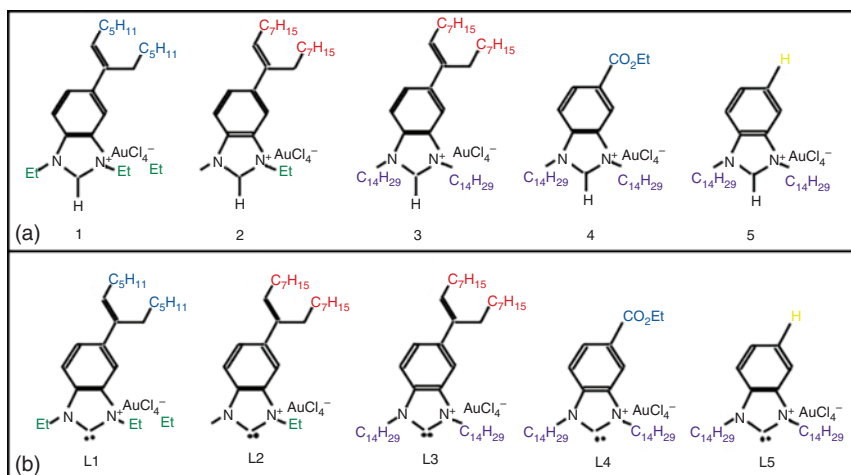


**Figure 1.17** Structures of NHC ligands 1–5 and deprotonated ligands (L1–L5) for Au nanocrystals. Source: Based on Refs. [76–80].

**Figure 1.18** Strategy for synthesizing NHC-coated Au nanocrystals by one-phase reduction of well-defined  $[(\text{NHC})\text{AuCl}]$  complexes.

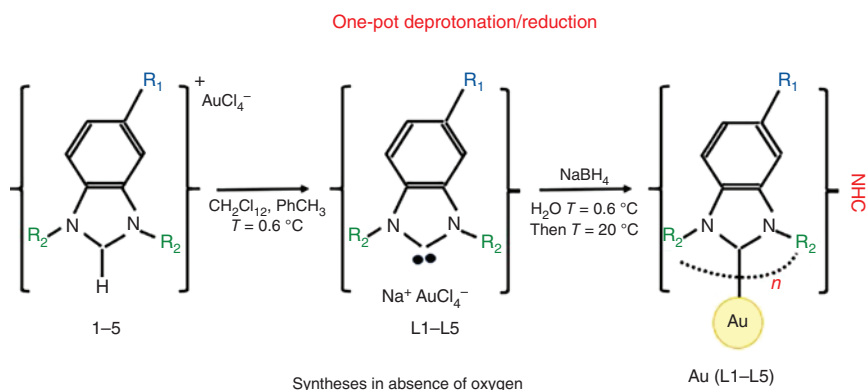
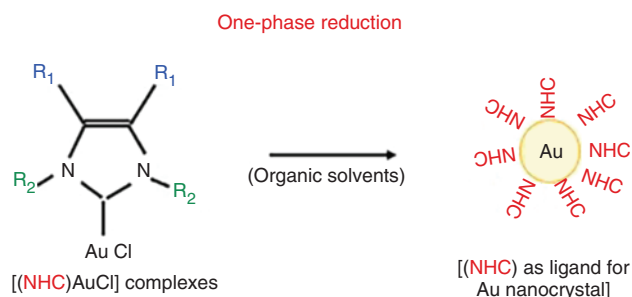


**Figure 1.19** Typical procedure for the preparation of NHC-coated Au nanocrystals (L1–L5@AuNC) from benzimidazolium chloroaurate salts (in a glove box).

- (ii) *One-pot deprotonation/reduction method*: to produce Au nanocrystals coated with various NHC ligands, a method based on deprotonation/reduction reaction of chloroaurate(III) imidazolium salts as precursors is used. In a previous study [91], well-defined metal–NHC complexes and air-sensitive NHC ligands are generated *in situ* and not isolated. This sequence gives large Au nanocrystals (16.6 nm) with a wide size distribution of  $\pm 49\%$  [91]. Here, benzimidazolium chloroaurate salts in which the heterocycle is functionalized by C<sub>7</sub>–C<sub>14</sub> long alkyl chains are used (Figure 1.17).

All the five salts, although differing in the length and position of the alkyl chains, are found to generate stabilized Au nanocrystals (**L1–L5@Au** nanocrystals) after treatment by NaH as the base and reduction by NaBH<sub>4</sub> at 0–1 °C. In brief, the synthetic route is shown in Figure 1.19: the chemical reaction takes place in a glove box. A suspension of sodium hydride in a 1 : 1 mixture of CH<sub>2</sub>Cl<sub>2</sub>/toluene is added to a solution of chloroaurate benzimidazolium salt in CH<sub>2</sub>Cl<sub>2</sub>. The mixture is stirred. A solution of NaBH<sub>4</sub> in water is added dropwise while maintaining the ice bath temperature. After addition, the mixture is stirred at room temperature. The solvents are removed under a nitrogen flow to give a dark powder. The powder is washed with ethanol and the suspension is centrifuged. The supernatant (EtOH) is removed. The residue is dried under a nitrogen stream to give Au nanocrystals as a dark powder. Table 1.2 shows that the size distribution, before size selection, is very wide. To reduce such distribution, size selection is based on a mixture of good and bad solvents. Table 1.2 shows that nanocrystals with narrower size distributions of 9–12% could successfully. The final **L1–L5@Au** nanocrystals are stable for weeks as clear purple-red colloidal solutions in toluene. By deposition of the colloidal solution, nanocrystals self-assemble in compact hexagonal network (Figure 1.20). The nanocrystal size changes with the ligand used and evolves from 3.5 to 6 nm (Table 1.2).

**Table 1.2** Summary of NHC-coated Au NC **L1–L5@Au** nanocrystal properties: average diameter (*d*) and size distribution (*σ* %).

Au nanocrystal	Before size selection		After size selection	
	<i>d</i> (nm)	<i>σ</i> (%)	<i>d</i> (nm)	<i>σ</i> (%)
L1 Au nanocrystals	5.9	13.3	6.0	9.2
L2 Au nanocrystals	5.7	20.4	5.7	11.2
L3 Au nanocrystals	3.5	19.9	4.0	11.9
L4 Au nanocrystals	5.4	16.4	5.2	10.2
L5 Au nanocrystals	4.7	15.5	5.0	10.1

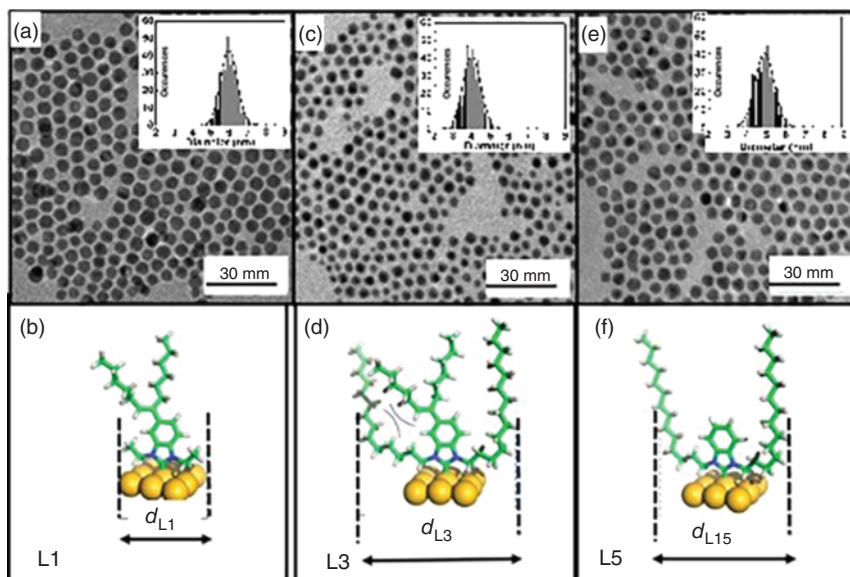


**Figure 1.20** TEM images and inset corresponding size distribution of Au nanocrystals coated with various N-heterocyclic carbenes. (a) nanocrystals coated with L1 (b), (c) nanocrystals coated with L3 (d), (e) nanocrystals coated with L5 (f). Source: Ling et al. [78]/American Chemical Society. Source: (a, c, e) Ling et al. [78]/American Chemical Society.

## 1.6 Conclusion

In this chapter, we described a very large number of methods to control metal nanocrystal sizes with a rather low size distribution. This favors to self-assemble nanocrystals in 2D and 3D superlattices. Furthermore, we find that, in some specific cases, it has been possible to control the crystalline structures of nanoparticles called nanocrystallinity. In the other chapters, we will discuss the importance of the nanocrystallinity on 3D superlattices.

## References

- 1 Pileni, M.P. (2003). Role of soft colloidal templates in the control of size and shape of inorganic nanocrystals. *Nat. Mater.* 2: 145–150.
- 2 Pileni, M.P. (1993). Reverse micelles as microreactors. *J. Phys. Chem.* 97: 6961–6973.
- 3 Sugimoto, T. (2001). *Monodispersed Particles*. Amsterdam: Elsevier.
- 4 Punties, V.F., Zanchet, D., Erdonmez, C.K., and Alivisatos, A.P. (2002). Synthesis of hcp nanodisks. *J. Am. Chem. Soc.* 124: 12874.
- 5 Prasad, B.L.V., Stoeva, S.I., Sorensen, C.M., and Klabunde, K.J. (2002). Digestive ripening of thiolated gold nanoparticles: the effect of alkyl chain length. *Langmuir* 18: 7515–7520.



- 6 Arbouet, A., Voisin, C., Christofilos, D. et al. (2003). Electron-phonon scattering in metal clusters. *Phys. Rev. Lett.* 90: 177401-1–177401-4.
- 7 Daniel, M.C. and Astruc, D. (2004). Gold nanoparticles: assembly, supramolecular chemistry, quantum size related properties and applications toward biology, catalysis, and nanotechnology. *Chem. Rev.* 104: 293–346.
- 8 Wang, J., Zhuang, Q., Peng, Y., and Li, A. (2005). A general strategy for nanocrystal synthesis. *Nature* 437: 121–124.
- 9 Kwon, S.G., Piao, Y., Park, J. et al. (2007). Kinetics of monodisperse iron oxide nanocrystal formation by “heating-up” process. *J. Am. Chem. Soc.* 129: 12571.
- 10 Kwon, S.G. and Hyeon, T. (2011). Formation mechanisms of uniform nanocrystals via hot-injection and heat-up methods. *Small* 7: 2685.
- 11 Kwon, S.G. and Hyeon, T. (2008). Colloidal chemical synthesis and formation kinetics of uniformly sized nanocrystals of metals, oxides, and chalcogenides. *Acc. Chem. Res.* 41: 1696–1709.
- 12 Robinson, I., Zacchini, S., Tung, L.D. et al. (2009). *Chem. Mater.* 21: 3021.
- 13 Goubet, N., Ding, Y., Brust, M. et al. (2009). A way to control the gold nanocrystals size: using seeds with different sizes and subjecting them to mild annealing. *ACS Nano* 3: 3622–3628.
- 14 Smith, D.K., Miller, N.R., and Korgel, B.A. (2009). Iodide in CTAB prevents gold nanorod formation. *Langmuir* 25 (16): 9518–9524.
- 15 Carbone, L. and Cozzoli, P.D. (2010). Colloidal heterostructured nanocrystals synthesis and growth mechanisms. *Nano Today* 5: 449.
- 16 Zhang, R., Khalizov, A., Wang, L. et al. (2012). Nucleation and growth of nanoparticles in the atmosphere. *Chem. Rev.* 112: 1957.
- 17 Taleb, A., Petit, C., and Pileni, M.P. (1997). Synthesis of highly monodisperse silver nanoparticles from AOT reverse micelles: a way to 2D and 3D self-organization. *Chem. Mater.* 9: 950–959.
- 18 Fievet, F., Ammar-Merah, S., Brayner, R. et al. (2018). The polyol process: a unique method for easy access to metal nanoparticles with tailored sizes, shapes and compositions. *Chem. Soc. Rev.* 47: 5187–5233.
- 19 LaMer, V.K. and Dinegar, R.H. (1950). Theory, production and mechanism of formation of monodispersed hydrosols. *J. Am. Chem. Soc.* 72: 4847.
- 20 LaMer, V.K. (1952). Nucleation in phase transition. *Ind. Eng. Chem.* 44: 1270.
- 21 Wu, N., Fu, L., Su, M. et al. (2004). Interaction of fatty acid monolayers with cobalt nanoparticles. *Nano Lett.* 4: 383–386.
- 22 Legrand, J., Petit, C., Bazin, D., and Pileni, M.P. (2000). Collective effect on magnetic properties of 2D superlattices of nanosized cobalt particles. *Appl. Surf. Sci.* 164: 186–192.
- 23 Love, J.C., Estroff, L.A., Kriebel, J.K. et al. (2005). Self-assembled monolayers of thiolates on metals as a form of nanotechnology. *Chem. Rev.* 105: 1103–1169.
- 24 Mourdikoudis, S. and Liz-Marzan, L.M. (2013). Oleylamine in nanoparticle synthesis. *Chem. Mater.* 25 (9): 1465–1476.
- 25 Shimpi, J.R., Sidhayee, D.S., and Prasad, B.L.V. (2017). Digestive ripening: a fine chemical machining process on the nanoscale. *Langmuir* 33: 9491–9507.

- 26 Zhang, S., Zhang, L., Liu, K. et al. (2018). Digestive ripening in the formation of monodisperse silver nanospheres. *Mat. Chem. Front.* 2: 1328–1333.
- 27 Irzhak, T.F. and Irzhak, V.I. (2019). On the digestive ripening mechanism. *Dokl. Phys. Chem.* 486: 77–79.
- 28 Scott, R.L. and Magat, M. (1945). The thermodynamics of high-polymer solutions: I. The free energy of mixing of solvents and polymers of heterogeneous distribution. *J. Chem. Phys.* 13: 172.
- 29 Burda, C., Chen, X.B., Narayanan, R., and El-Sayed, M.A. (2005). Chemistry and properties of nanocrystals of different shapes. *Chem. Rev.* 105: 1025–1102.
- 30 Baletto, F. and Ferrando, R. (2005). Structural properties of nanoclusters: energetic, thermodynamic and kinetic effects. *Rev. Mod. Phys.* 77: 371–423.
- 31 Baletto, F., Mottet, C., and Ferrando, R. (2001). Microscopic mechanisms of the growth of metastable silver icosahedra. *Phys. Rev. B* 63: 155408.
- 32 Baletto, F., Mottet, C., and Ferrando, R. (2000). Reentrant morphology transition in the growth of free silver nanoclusters. *Phys. Rev. Lett.* 84: 5544–5547.
- 33 Park, J., Joo, J., Kwon, S.G. et al. (2007). Synthesis of monodisperse spherical nanocrystals. *Angew. Chem. Int. Ed.* 46: 4630–4660.
- 34 Yin, Y. and Alivisatos, A.P. (2005). Colloidal nanocrystal synthesis and the organic–inorganic interface. *Nature* 437: 664–670.
- 35 Dinega, D.P. and Bawendi, M.G. (1999). A solution-phase chemical approach to a new crystal structure of cobalt. *Angew. Chem.* 38: 1788–1791.
- 36 Sun, S.H., Murray, C.B., Weller, D. et al. (2000). Monodisperse FePt nanoparticles and ferromagnetic FePt nanocrystal superlattices. *Science* 287: 1989.
- 37 Kirkland, A.I., Jefferson, D.A., Duff, D.G. et al. (1993). Structural studies of trigonal lamellar particles of gold and silver. *Proc. R. Soc. Lond. A* 440: 589–609.
- 38 Schadt, M., Cheung, W., Luo, J., and Zhong, C.J. (2006). Molecularly tuned size selectivity in thermal processing of gold nanoparticles. *Chem. Mater.* 18: 5147–5150.
- 39 Shimizu, T., Terashini, T., Hasegawa, S., and Miyake, M.J. (2003). Size evolution of alkanethiol-protected gold nanoparticles by heat treatment in the solid state. *J. Phys. Chem. B* 107: 2719–2724.
- 40 Beck, C.G.S., Souza, T.L., Silva, M. et al. (2011). Formation mechanism via a heterocoagulation approach of FePt nanoparticles using the modified polyol process. *J. Phys. Chem. C* 115: 10475–10482.
- 41 Petit, C. and Pileni, M.P. (1988). Synthesis in situ of cadmium sulfite synthesized in reverse micelles and hydrocarbon gels. *J. Phys. Chem.* 92: 2282–2286.
- 42 Petit, C., Lixon, P., and Pileni, M.P. (1990). Synthesis in situ of cadmium sulfate semiconductor: 2. Effect of functionalized surfactant. *J. Phys. Chem.* 94: 1598–1603.
- 43 Petit, C., Lixon, P., and Pileni, M.P. (1993). Synthesis in situ of silver nanocluster in AOT reverse micelles. *J. Phys. Chem.* 97: 12974–12983.
- 44 Pileni, M.P. (1997). Nanosized particles made in colloidal assemblies. *Langmuir* 13: 3266–3276.
- 45 Pileni, M.P. (2001). Mesosstructured fluids in oil rich regions: structural and templating approaches. *Langmuir* 17: 7476–7487.

- 46 Lisiecki, I. and Pileni, M.P. (2003). Synthesis of well-defined and low size distribution cobalt nanocrystals: the limited influence of reverse micelles. *Langmuir* 19: 9486.
- 47 Cavalier, M., Wall, M., Lisiecki, I., and Pileni, M.P. (2011). How can the nanocrystallinity of 7 nm spherical Co nanoparticles dispersed in solution be improved? *Langmuir* 27: 5014–5020.
- 48 Yang, Z., Cavalier, M., Walls, M. et al. (2012). A phase-solution annealing strategy to control the cobalt nanocrystal anisotropy: structural and magnetic investigations. *J. Phys. Chem. C* 116: 15723–15730.
- 49 Pileni, M.P., Zemb, T., and Petit, C. (1985). Solubilization by reverse micelles: solute localization and structure perturbation. *Chem. Phys. Lett.* 118: 414.
- 50 Yang, N., Yang, J., Yang, J. et al. (2015). Control of the oxygen and cobalt atoms diffusion through Co nanoparticles differing by their crystalline structure and size. *Adv. Funct. Mater.* 25: 891–897.
- 51 Wei, J., Schaeffer, N., Albouy, P.A., and Pileni, M.P. (2015). Surface plasmon resonance properties of silver nanocrystals differing in size and coating agent ordered in 3D supracrystals. *Chem. Mater.* 27: 5614–5621.
- 52 Maye, M.M., Zheng, W., Leibowitz, F.L. et al. (2000). Heating-induced evolution of thiolate-encapsulated gold nanoparticles: a strategy for size and shape manipulations. *Langmuir* 16: 490–497.
- 53 Zheng, N., Fan, J., and Stucky, G.D. (2006). One-step one-phase synthesis of monodisperse noble-metallic nanoparticles and their colloidal crystals. *J. Am. Chem. Soc.* 128: 6550–6551.
- 54 Goubet, N., Portalès, H., Yan, C. et al. (2012). Simultaneous growths of gold colloidal crystals. *J. Am. Chem. Soc.* 134: 3714–3719.
- 55 Goubet, N., Richardi, J., Albouy, P.A., and Pileni, M.P. (2011). Which forces do control the supracrystal nucleation in organic media. *Adv. Funct. Mater.* 21: 2693–2704.
- 56 Portalès, H., Goubet, N., Saviot, L. et al. (2010). Crystallinity dependence of the plasmon resonant Raman scattering by anisotropic gold nanocrystals. *ACS Nano* 4: 3490–3497.
- 57 Goubet, N., Tempira, I., Yang, J. et al. (2015). Size and nanocrystallinity controlled gold nanocrystals: synthesis, electronic and mechanical properties. *Nanoscale* 7: 3237–3246.
- 58 Portalès, H., Goubet, N., Saviot, L. et al. (2008). Probing atomic ordering and multiple twinning in metal nanocrystals through their vibrations. *Proc. Natl. Acad. Sci. USA* 105: 14784–14789.
- 59 Peng, S., Xie, J., and Sun, S. (2008). Synthesis of Co/MFe<sub>2</sub>O<sub>4</sub> (M = Fe, Mn) core/shell nanocomposite particles. *J. Solid State Chem.* 181: 1560.
- 60 Yang, Z., Wei, J., Bonville, P., and Pileni, M.P. (2015). Engineering the magnetic dipolar interactions in three-dimensional binary supracrystals via mesoscale alloying. *Adv. Funct. Mater.* 25: 4908.
- 61 Yang, Z., Yang, J., Bergström, J. et al. (2014). Crystal polymorphism: dependence of oxygen diffusion through 2D ordered Co nanocrystals. *Phys. Chem. Chem. Phys.* 16: 9791–9796.

- 62 Yang, J., Khazen, K., and Pileni, M.P. (2014). How nanocrystallinity and order define the magnetic properties of e-Co supracrystal. *J. Phys. Condens. Matter* 26: 295303.
- 63 Wei, J., Schaeffer, N., and Pileni, M.P. (2016). Solvent-mediated crystallization of nanocrystal 3D assemblies of silver nanocrystals: unexpected superlattice ripening. *Chem. Mater.* 28: 293–302.
- 64 Williams, J.V., Kotov, N.A., and Savage, P.E. (2009). A rapid hot-injection method for the improved hydrothermal synthesis of CdSe nanoparticles. *Ind. Eng. Chem. Res.* 48 (9): 4316–4321.
- 65 Timonen, J.V.I., Seppala, E.T., Ikkala, O., and Ras, R.H.A. (2011). From hot-injection synthesis to heating-up synthesis of cobalt nanoparticles: observation of kinetically controllable nucleation. *Angew. Chem. Int. Ed.* 50: 2080–2084.
- 66 Brust, M., Walker, M., Bethell, D. et al. (1994). Synthesis of thiol-derivatized gold nanoparticles in a two-phase liquid/liquid system. *J. Chem. Soc., Chem. Commun.* 801–802.
- 67 Brust, M., Fink, J., Bethell, D. et al. (1995). Synthesis and reactions of functionalised gold nanoparticle. *J. Chem. Soc., Chem. Commun.* 1655–1656.
- 68 Zhou, M., Chen, S., and Zhao, S. (2006). Synthesis of icosahedral gold nanocrystals: a thermal process strategy. *J. Phys. Chem. B* 110: 4510–4513.
- 69 Chushak, Y.G. and Bartell, L.S. (2001). Melting and freezing of gold nanoclusters. *J. Phys. Chem. B* 105: 11605.
- 70 Nam, H.S., Hwang, N.M., Yu, B.D., and Yoon, J.K. (2002). Formation of an icosahedral structure during the freezing of gold nanoclusters: surface-induced mechanism. *Phys. Rev. Lett.* 89: 275502-1–275502-4.
- 71 Shim, J.H., Lee, B.J., and Cho, Y.W. (2002). Thermal stability of unsupported gold nanoparticle: a molecular dynamics study. *Surf. Sci.* 512: 262–268.
- 72 Bourissou, D., Guerret, O., Gabbai, F.P., and Bertrand, G. (2000). Stable carbenes. *Chem. Rev.* 100: 39–92.
- 73 Herrmann, W.A. (2002). N-Heterocyclic carbenes: a new concept in organometallic catalysis. *Angew. Chem. Int. Ed.* 41: 1290–1309.
- 74 Hahn, F.E. and Jahnke, M.C. (2008). Heterocyclic carbenes: synthesis and coordination chemistry. *Angew. Chem. Int. Ed.* 47: 3122–3172.
- 75 Hopkinson, M.N., Richter, C., Schedler, M., and Glorius, F. (2014). An overview of N-heterocyclic carbenes. *Nature* 510: 485–496.
- 76 Ling, X., Schaeffer, N., Roland, S., and Pileni, M.P. (2013). Nanocrystals: why do silver and gold N-heterocyclic carbene precursors behave differently? *Langmuir* 29: 12647–12656.
- 77 Ling, X., Roland, S., and Pileni, M.P. (2015). Superior oxygen stability of N-heterocyclic carbene-coated Au nanocrystals. *Langmuir* 31: 12873–12882.
- 78 Ling, X., Roland, S., and Pileni, M.P. (2015). Supracrystals of N-heterocyclic carbene-coated Au nanocrystals. *Chem. Mater.* 27: 414–423.
- 79 Ling, X. (2015). Unpublished experiments. PhD thesis. UPMC-University, Paris.
- 80 Roland, S., Ling, X., and Pileni, M.P. (2016). N-Heterocyclic carbene ligands for Au nanocrystal stabilization and three-dimensional self-assembly. *Langmuir* 32: 7683–7696.

- 81 Ott, L.S., Cline, M.L., Deetlefs, M. et al. (2005). Nanoclusters in ionic liquids: evidence for N-heterocyclic carbene formation from imidazolium-based ionic liquids detected by  $^2\text{H}$  NMR. *J. Am. Chem. Soc.* 127: 5758–5759.
- 82 Scholten, J.D., Ebeling, G., and Dupont, J. (2007). On the involvement of NHC carbenes in catalytic reactions by iridium complexes, nanoparticle and bulk metal dispersed in imidazolium ionic liquids. *Dalton Trans.* 5554–5560.
- 83 Huang, R.T.W., Wang, W.C., Yang, R.Y. et al. (2009). Liquid crystals of gold(I) N-heterocyclic carbene complexes. *Dalton Trans.* 7121–7131.
- 84 Hurst, E.C., Wilson, K., Fairlamb, I.J.S., and Chechik, V. (2009). N-Heterocyclic carbene coated metal nanoparticles. *New J. Chem.* 33: 1837–1840.
- 85 Vignolle, J. and Tilley, T.D. (2009). N-Heterocyclic carbene-stabilized gold nanoparticles and their assembly into 3D superlattices. *Chem. Commun.* 7230–7232.
- 86 Aslanov, L.A., Zakharov, V.N., Zakharov, M.A. et al. (2010). Stabilization of silicon nanoparticles by carbenes. *Russ. J. Coord. Chem.* 36: 330–332.
- 87 Kang, J.N., Yang, H.Y., Kim, H.I., and Son, S.U. (2010). Colloidal synthesis of cubic-phase copper selenide nanodiscs and their optoelectronic properties. *Chem. Mater.* 22: 3586–3588.
- 88 Ranganath, K.V.S., Kloesges, J., Schäfer, A.H., and Glorius, F. (2010). Asymmetric nanocatalysis: N-heterocyclic carbenes as chiral modifiers of  $\text{Fe}_3\text{O}_4/\text{Pd}$  nanoparticles. *Angew. Chem. Int. Ed.* 49: 7786–7789.
- 89 Lara, P., Rivada-Wheelaghan, O., Conejero, S. et al. (2011). Ruthenium nanoparticles stabilized by N-heterocyclic carbenes: ligand location and influence on reactivity. *Angew. Chem. Int. Ed.* 50: 12080–12084.
- 90 Gonzales-Galves, D., Lara, P., Rivada-Wheelaghan, O. et al. (2013). NHC-stabilized ruthenium nanoparticles as new catalysts for the hydrogenation of aromatics. *Catal. Sci. Technol.* 3: 99–105.
- 91 Serpell, C.J., Cookson, J., Thompson, A.L. et al. (2013). Haloaurate and halopalladate imidazolium salts: structures, properties, and use as precursors for catalytic metal nanoparticles. *Dalton Trans.* 42: 1385–1393.
- 92 Baquero, E.A., Tricard, S., Flores, J.C. et al. (2014). Highly stable water-soluble platinum nanoparticles stabilized by hydrophilic N-heterocyclic carbenes. *Angew. Chem. Int. Ed.* 53: 13220–13224.
- 93 Song, S.G., Satheeshkumar, C., Park, J. et al. (2014). N-Heterocyclic carbene-based conducting polymer–gold nanoparticle hybrids and their catalytic application. *Macromolecules* 47: 6566–6571.
- 94 Liu, H.X., He, X., and Zhao, L. (2014). Metallamacrocycle-modified gold nanoparticles: a new pathway for surface functionalization. *Chem. Commun.* 50: 971–974.
- 95 Richter, C., Schaepe, K., Glorius, F., and Ravoo, B.J. (2014). Tailor-made N-heterocyclic carbenes for nanoparticle stabilization. *Chem. Commun.* 50: 3204–3207.
- 96 Rodriguez-Castillo, M., Laurencin, D., Tielens, F. et al. (2014). Reactivity of gold nanoparticles towards N-heterocyclic carbenes. *Dalton Trans.* 43: 5978–5982.

- 97 Crespo, J., Guari, Y., Ibarra, A. et al. (2014). Ultrasmall NHC-coated gold nanoparticles obtained through solvent free thermolysis of organometallic Au(I) complexes. *Dalton Trans.* 43: 15713–15718.
- 98 MacLeod, M.J. and Johnson, J.A. (2015). PEGylated N-heterocyclic carbene anchors designed to stabilize gold nanoparticles in biologically relevant media. *J. Am. Chem. Soc.* 137: 7974–7977.
- 99 Ferry, A., Schaepe, K., Tegeder, P. et al. (2015). Negatively charged N-heterocyclic carbene-stabilized Pd and Au nanoparticles and efficient catalysis in water. *ACS Catal.* 5: 5414–5420.
- 100 Zhukhovitskiy, A.V., MacLeod, M.J., and Johnson, J.A. (2015). Carbene ligands in surface chemistry: from stabilization of discrete elemental allotropes to modification of nanoscale and bulk substrates. *Chem. Rev.* 115: 11503–11532.
- 101 Weidner, T., Baio, J.E., Mundstock, A. et al. (2011). NHC-based self-assembled monolayers on solid gold substrates. *Aust. J. Chem.* 64: 1177–1179.
- 102 Zhukhovitskiy, A.V., Mavros, M.G., Van Voorhis, T., and Johnson, J.A. (2013). Addressable carbene anchors for gold surfaces. *J. Am. Chem. Soc.* 135: 7418–7421.
- 103 Crudden, C.M., Horton, J.H., Ebraldze, I.I. et al. (2014). Ultra stable self-assembled monolayers of N-heterocyclic carbenes on gold. *Nat. Chem.* 6: 409–414.
- 104 Benhamou, L., Chardon, E., Lavigne, G. et al. (2011). Synthetic routes to N-heterocyclic carbene precursors. *Chem. Rev.* 111: 2705–2733.
- 105 Nelson, D.J. and Nolan, S.P. (2013). Quantifying and understanding the electronic properties of N-heterocyclic carbenes. *Chem. Soc. Rev.* 42: 6723–6753.
- 106 Pykkö, P. and Runeberg, N. (2006). Comparative theoretical study of N-heterocyclic carbenes and other ligands bound to Au<sup>I</sup>. *Chem. Asian J.* 1: 623–628.
- 107 Yang, Z., Lisiecki, I., Walls, M., and Pileni, M.P. (2013). Nanocrystallinity and the ordering of nanoparticles in 2D superlattices: controlled formation of either core/shell (Co/CoO) or hollow CoO nanocrystals. *ACS Nano* 7: 1342–1350.